Supplement of Geosci. Model Dev., 15, 1971–1994, 2022
https://doi.org/10.5194/gmd-15-1971-2022-supplement

Geoscientific Model Development
Open Access
EGU

Supplement of

Global evaluation of the Ecosystem Demography model (ED v3.0)

Lei Ma et al.

Correspondence to: Lei Ma (lma6@umd.edu)

This supplement includes two parts. The first part describes equations and parameters of each submodule of ED (v3.0) (S1 - S11). For most modules, the descriptions are based on Moorcroft et al., (2001), Hurtt et al., (2002) and Albani et al., (2006) and updated as appropriate. The second part includes supplement figures.

S1. Plant functional type

In ED, we refine PFTs previously developed in Moorcroft et al., (2001), Hurtt et al., (2002) and Albani et al., (2006). Here we include seven major types, namely early-successional broadleaf trees (EaSBT), middle-successional broadleaf trees (MiSBT), late-successional broadleaf trees (LaSBT), northern and southern pines (NSP), late-successional conifers (LaSC), C3 shrubs and grasses (C3ShG), and C4 shrubs and grasses (C4ShG). The broadleaf PFTs (i.e., EaSBT, MiSBT, and LaSBT) are further distinguished between tropical and non-tropical subtypes in terms of leaf traits (e.g., leaf lifespan, specific leaf area, and leaf photosynthesis rate) and mortality rate. The geographic boundary of tropical and non-tropical subtypes is delineated by whether the multi decade average air temperature during the coldest month of the year is above or below 18 °C.

These PFTs primarily differ in their phenology, leaf physiological traits, allometry, mortality rate, and dispersal distance. Regarding their phenology, needleleaf PFTs (i.e., NSP and LaSC) are evergreen, and broadleaf PFTs (both tropical and non-tropical subtypes) and grass PFTs are cold-deciduous and drought-deciduous. For leaf traits, broadleaf tropical subtypes have longer lifespans but lower average specific leaf area and carboxylation rates than non-tropical subtypes. Needleleaf PFTs have longer lifespan than broadleaf PFTs, and grass and shrub PFTs have the shortest leaf lifespans (less than 1 year). The seven major PFTs all use different allometric equations, but broadleaf PFT subtypes share the same allometry, and grass and shrub PFTs are limited terms of maximum height. Grass PFTs have the highest mortality rates, followed by broadleaf PFTs and needleleaf PFTs. Dispersal distance also varies across PFTs, where the EaSBT disperses more seedlings to non-local patches than either the MiSBT and LaSBT, and the NSP is more than the LaSC. All PFTs are differentiated by their photosynthetic pathways and C3 and C4 photosynthesis processes are modelled separately (see later discussion in S3 on the leaf physiology submodule). Moreover, needleleaf PFTs are characterized by slower leaf and root decay rates than broadleaf PFTs and also utilize different allometry equations. Here, broadleaf trees are split into early-, mid- and late-successional types, which differ not only in terms of their leaf and root decay rates but also in wood density and respective allometry. The empirical relationship between leaf nitrogen content and leaf longevity, and the relationship between specific leaf area and leaf longevity, follow Moorcroft et al., 2001, which follows Reich et al., 1997.

Spatial distribution of PFTs is mechanistically determined by individual competition for light, water, and nutrients. No quasi-equilibrium climate–vegetation relationships, such as satellite-based PFT maps or climatic envelope thresholds, are used to constrain presence or absence of PFTs. All PFTs could potentially coexist in any location over the globe and are initialized with the same density; the subsequent competition determines when and where specific PFTs dominate the ecosystems. The competitive advantage of each PFT results from plant traits such as photosynthesis efficiency, height growth rate, and reproduction strategies. These advantages vary with climate

conditions and across stages of ecosystem succession. For example, leaf physiological traits exhibit trade-offs across PFTs (Reich et al., 1997). Compared to needleleaf PFTs, broadleaf PFTs have a relatively larger leaf area per leaf weight and higher carbon assimilation rate per leaf area, but higher carbon demand for leaf turnover. Moreover, the early-successional PFT rapidly accumulates carbon, quickly grows in height, and disperses seeds over long distances. These characteristics lead to its dominance during the early successional state of recently disturbed ecosystems. However, its intolerance of shade makes it less competitive as the canopy closes, eventually being replaced by mid- and late-successional PFTs which have lower morality in shade but grow more slowly in height.

Table S1.1. Summary of PFT-dependent parameters. V_{cmax} is used in the leaf physiology submodule; $\rho(x)$, DBH_{max}, a_h, b_h, a_l, b_l, a_s, b_s, $l(x)$, $\alpha_l(x)$ and $\beta_r(x)$ are used in the plant allocation submodule; $m(x)$ is used in reproduction; *phenology*, $T_{crit}(x)$ and $T_{free}(x)$ are used in the leaf phenology and freezing submodule; and $\mu_{DI}(x)$ is used in the mortality submodule. Note that C4ShG is C4 shrubs and grasses, C3ShG is C3 shrubs and grasses, EaSBT is early-successional broadleaf trees, MiSBT is middle-successional broadleaf trees, LaSBT is late-successional broadleaf trees, NSP is northern and southern pines, and LaSC is late-successional conifers. TRO and NTRO are tropical and non-tropical variants of EaSBT, MiSBT, LaSBT.

Parameters	**Description**	**C4ShG**	**C3ShG**	**EaSBT**		**MiSBT**		**LaSBT**		**NSP**	**LaSC**
				TRO	NTRO	TRO	NTRO	TRO	NTRO		
V_{cmax}	Maximum rate of Rubisco carboxylation (μ mol m^{-2} s^{-1})	20	80	50	60	45	55	40	50	21	19
$\rho(x)$	Wood density (g cm^{-3})	0.53	0.53	0.53	0.53	0.71	0.71	0.90	0.90	0.70	0.70
DBH_{max}	Corresponding DBH at maximum canopy height (cm)	0.35	0.35	68.31	68.31	68.31	68.31	68.31	68.31	42.09	42.09
a_h	Coefficient of height allometry	-	-	-	-	-	-	-	-	27.14	22.19
b_h	Coefficient of height allometry	-	-	-	-	-	-	-	-	-0.0388	-0.0445
a_l	Coefficient of leaf biomass allometry	-	-	-	-	-	-	-	-	0.024	0.045
b_l	Coefficient of leaf biomass allometry	-	-	-	-	-	-	-	-	1.899	1.683
a_s	Coefficient of structural biomass allometry	-	-	-	-	-	-	-	-	0.147	0.162
b_s	Coefficient of structural biomass allometry	-	-	-	-	-	-	-	-	2.238	2.154
$l(x)$	Specific leaf area (m^2 kg^{-1} C)	22.03	22.03	16.02	28.50	11.64	26.55	9.66	24.42	5.55	5.55
$\alpha_l(x)$	Leaf biomass decay rate (yr^{-1})	2.0	2.0	1.0	3.5	0.5	3.0	0.33	2.5	0.1	0.1
$\alpha_r(x)$	Fine root decay rate (yr^{-1})	2.0	2.0	1.0	0.1	0.5	0.1	0.33	0.1	0.1	0.1
$\beta_r(x)$	Respiration coefficient	0.2	0.2	0.2	0.2	0.2	0.2	0.2	0.2	0.2	0.2

$m(x)$	Non-local dispersal rate	1.0	1.0	1.0	1.0	0.5	0.5	0.2	0.2	0.78	0.2
phenology	C-cold deciduous D-drought-deciduous E-evergreen	C, D	C, D	C, D	C, D	C, D	C, D	C, D	C, D	E	E
$T_{crit}(x)$	Temperature threshold triggering leaf drop (°C)	15	5	10	10	10	10	10	10	-	-
$T_{free}(x)$	Temperature threshold of freezing resistance (°C)	-	-	-15	-15	-15	-15	-15	-15	-80	-80
$\mu_{_{DI}}(x)$	Density independent mortality (yr^{-1})	0.081	0.081	0.081	0.032	0.054	0.032	0.025	0.014	0.014	0.014

S2. Plant allocation submodule

Regardless of PFT type, each individual plant consists of both active tissue (B_a) and structural tissue (B_s). B_a includes leaf biomass (B_l), sapwood biomass (B_{sw}), and fine root biomass (B_r). The biomass in each active tissue component governs plant functioning. For example, leaf biomass determines the number of leaves available for photosynthesis, and the fine root biomass determines the amount of water uptake from soil. Distribution of B_a to B_l, B_{sw} , and B_r is based on ratio factors of $q_l(\mathbf{z},\mathbf{x})$, $q_r(\mathbf{z},\mathbf{x})$ and $q_{sw}(\mathbf{z},\mathbf{x})$, respectively. Assuming B_l and B_r are equal for all PFTs, and the sapwood cross-sectional area is proportional to total leaf area, then $q_l(\mathbf{z},\mathbf{x})$, $q_r(\mathbf{z},\mathbf{x})$ and $q_{sw}(\mathbf{z},\mathbf{x})$ are given by:

$$q_l(\mathbf{z},\mathbf{x}) = \frac{B_l}{B_a} = \frac{1}{2 + 0.00128l(\mathbf{x})h} \quad \text{Eq. S2.1}$$

$$q_r(\mathbf{z},\mathbf{x}) = \frac{B_r}{B_a} = \frac{1}{2 + 0.00128l(\mathbf{x})h} \quad \text{Eq. S2.2}$$

$$q_{sw}(\mathbf{z},\mathbf{x}) = \frac{B_{sw}}{B_a} = \frac{0.00128l(\mathbf{x})h}{2 + 0.00128l(\mathbf{x})h} \quad \text{Eq. S2.3}$$

Where $l(\mathbf{x})$ is dependent on PFT-specific leaf area, and h is plant height.

When the plant maintains a positive carbon balance, after taking into account respiration and decay costs from carbon fixation by photosynthesis, the gained carbon will be allocated towards the growth of B_a and B_s. The allocation fraction to B_a, defined as $q_a(\mathbf{z},\mathbf{x})$, is based on empirical allometry equations, which ensure B_a and B_s stay on a given allometric trajectory. However, a negative carbon balance in the plant could result in B_a departing from its allometric trajectory as B_a needs to decrease in order to compensate for respiration and decay costs. In this case, subsequent carbon gains will all be allocated to B_a until it resumes its allometry (i.e., $q_a(\mathbf{z},\mathbf{x}) = 1$).

Empirical allometry equations depict the relationship between plant height (h), leaf biomass (B_l) structural tissue (B_s), and Diameter at Breast Height (DBH). For broadleaf PFTs and grass and shrub PFTs, the allometry equations from Moorcroft et al., 2001 are used:

$$h = \begin{cases} 2.34DBH^{0.64} & if\ (DBH \leq\ DBH_{max}) \\ 2.34{DBH_{max}}^{0.64} & if\ (DBH >\ DBH_{max}) \end{cases} \quad \text{Eq. S2.4}$$

$$B_l = \begin{cases} 0.0419DBH^{1.56}\rho(\mathbf{x})^{0.55} & if\ (DBH \leq\ DBH_{max}) \\ 0.0419{DBH_{max}}^{1.56}\rho(\mathbf{x})^{0.55} & if\ (DBH >\ DBH_{max}) \end{cases} \quad \text{Eq. S2.5}$$

$$B_s = \begin{cases} 0.069h^{0.572}DBH^{1.94}\rho(\mathbf{x})^{0.931} & if\ (DBH \leq\ DBH_{max}) \\ 0.069{h_{max}}^{0.572}DBH^{1.94}\rho(\mathbf{x})^{0.931} & if\ (DBH >\ DBH_{max}) \end{cases} \quad \text{Eq. S2.6}$$

Where DBH_{max} is the corresponding DBH when h reaches its max (note that this is not the maximum DBH the plant can grow), and $\rho(\mathbf{x})$ is PFT-dependent wood density.

For the PFTs of NSP and LaSC, the allometry equations from Albani et al., 2006 are used:

$$h = 1.3 + a_h(1 - e^{b_h DBH}) \quad \text{Eq. S2.7}$$

$$B_l = \begin{cases} a_l DBH^{b_l} & if\ (DBH \leq\ DBH_{max}) \\ a_l {DBH_{max}}^{b_l} & if\ (DBH \leq\ DBH_{max}) \end{cases} \quad \text{Eq. S2.8}$$

$$B_s = a_s DBH^{b_s} \quad \text{Eq. S2.9}$$

Where a_h, b_h, a_l, b_l, a_s and b_s are allometry coefficients.

With ratio q_l from Eq. S2.1 and leaf biomass calculated from Eq. S2.5 or S2.8, the active tissue biomass on the allometric trajectory is:

$$B_a^{opt} = q_l(\mathbf{z}, \mathbf{x}) B_l^* \quad \text{Eq. S2.10}$$

Thus, when the plant is in positive carbon balance and B_a is not smaller than B_a^{opt}, the allocation fraction of new carbon to B_a is calculated as:

$$q_a(\mathbf{z}, \mathbf{x}) = \frac{\frac{dB_a^{opt}}{dB_s}(B_s)}{1 + \frac{dB_a^{opt}}{dB_s}(B_s)} \quad \text{Eq. S2.11}$$

S3. Leaf physiology submodule

The leaf physiology submodule estimates leaf-level photosynthesis and transpiration rates as key inputs to other submodules (e.g., growth and hydrological submodules). This submodule uses light, CO_2, air temperature, and air humidity as environmental inputs, and generates carbon assimilation and transpiration per leaf area as outputs. Three processes are coupled in this submodule: 1) photosynthesis, which describes carbon assimilation with consideration of light availability, leaf temperature, air humidity, and CO_2 supply; 2) stomatal conductance, which describes CO_2 diffusion from ambient air to leaf intercellular space and associated water vapor loss; and 3) leaf energy balance, which describes the energy budget (i.e., absorbed radiation, emitted thermal radiation, and sensible and latent heat loss) for each leaf and determines leaf temperature.

S3.1. Photosynthesis process

Photosynthesis processes are separately modelled for C3 and C4 PFTs. The Farquhar, von Caemmerer & Berry model (Farquhar et al., 1980) is used to describe the C3 photosynthetic pathway. When soil moisture and nutrients are not limited, net photosynthesis rate per unit leaf area is the difference between the gross photosynthesis rate, A, and mitochondrial respiration, R_d. As shown in Eq. S3.1, the gross photosynthesis rate is co-limited by three processes: (1) Rubisco-limited photosynthesis rate (A_c); (2) Light-limited or RuBP regeneration-limited photosynthesis rate (A_j); and (3) Product-limited or triose phosphate utilization-limited photosynthesis rate (A_e).

$$A_n = A - R_d = \left(A_c, A_j, A_e\right) - R_d \quad \text{Eq. S3.1}$$

The Rubisco-limited photosynthesis rate, A_c , is given by:

$$A_c = \frac{V_{cmax}(c_i - \Gamma^*)}{\left[c_i + K_c\left(1 + \frac{o_i}{K_o}\right)\right]} \quad \text{Eq. S3.2}$$

where V_{cmax} is the maximum rate of Rubisco carboxylation, c_i and o_i are the intercellular concentrations of CO_2, and O_2, respectively, Γ^* is the CO_2 compensation point, and K_c and K_o are the Michaelis-Menten constants of Rubisco for CO_2 and O_2, respectively. The RuBP regeneration-limited photosynthesis rate A_j is given by:

$$A_j = \frac{J(c_i - \Gamma^*)}{4(c_i + 2\Gamma^*)} \quad \text{Eq. S3.3}$$

Where J is the electron transport rate and given by:

$$\theta J^2 - (I_{PSII} + J_{max})J + I_{PSII}J_{max} = 0 \quad \text{Eq. S3.4}$$

$$I_{PSII} = \frac{1 - f}{2}\alpha I \quad \text{Eq. S3.5}$$

$$I = 4.55 \cdot \phi I_{g0} e^{-f_{sha}K_L \int_h^\infty L_{ttl}(h)}\, \xi \quad \text{Eq. S3.6}$$

In Eq. S3.4, θ is the curvature of the light response curve, I_{PSII} is the light utilized in electron transport by photosystem II, and J_{max} is the maximum rate of electron transport. In Eq. S3.5, α is leaf absorbance (set at 0.85), and f is the correction factor for spectral light quality (set at 0.15). In Eq. S3.6, I is incident photosynthetically active radiation (PAR, in unit of $\mu mol\ m^{-2}\ s^{-1}$) at leaf level with height h, I_{g0} is total shortwave radiation at the patch's canopy top, f_{sha} is the degree of shading, and K_L is light extinction coefficient. $L_{ttl}(h)$ is cumulative LAI

from the canopy top to leaf height, calculated by summing the leaf area of all cohort plants higher than h. ξ is a coefficient representing the proportion of PAR in shortwave radiation.

The export-limited photosynthesis rate (A_e) is related to the rate of triose phosphate utilization (T_p), and it is given by:

$$A_e = 3 \cdot T_p \quad \text{Eq. S3.7}$$

A model from von Caemmerer et al., 1999 is used to describe C4 photosynthesis. When soil moisture and nutrients are not limited, net photosynthesis rate per unit leaf area is the difference between A and R_d. The gross photosynthesis rate (A) is co-limited by: (1) Enzyme-limited photosynthesis rate (A_c) and (2) Light- and electron transport-limited photosynthesis rate (A_j).

$$A_n = A - R_d = \left(A_c, A_j\right) - R_d \quad \text{Eq. S3.8}$$

The enzyme-limited photosynthesis rate (A_c) is given by solving a quadratic equation:

$$a{A_c}^2 + bA_c + c = 0 \quad \text{Eq. S3.9}$$

Where

$$a = 1 - \frac{\alpha_o}{0.047}\frac{K_c}{K_o} \quad \text{Eq. S3.10}$$

$$b = -\left\{\left(\left(V_p - R_m + g_{bs}C_m\right) + \left(V_{cmax} - R_d\right) + g_{bs}K_c\left(1 + \frac{O_m}{K_o}\right)\right) + \left(\frac{\alpha_o}{0.047}\left(\gamma_* V_{cmax} + R_d\frac{K_c}{K_o}\right)\right)\right\} \quad \text{Eq. S3.11}$$

$$c = \left(V_{cmax} - R_d\right)\left(V_p - R_m + g_{bs}C_m\right) - \left(V_{cmax}g_{bs}\gamma_* O_m + R_d g_{bs}K_c\left(1 + \frac{O_m}{K_o}\right)\right) \quad \text{Eq. S3.12}$$

Where α_o in Eq. S3.10 is the fraction of PSII activity in the bundle sheath. In Eq. S3.11 and S3.12, C_m and O_m are the partial pressure of CO_2 and O_2 in the mesophyll, C_m equals the CO_2 intercellular partial pressure (C_i), if assuming mesophyll conductance, is infinite. g_{bs} is bundle sheath conductance to CO_2, R_m is mesophyll mitochondrial respiration, and γ_* is half of the reciprocal of Rubisco specificity. V_p is the rate of phosphoenolpyruvate (PEP) carboxylation, given by:

$$V_p = min\left\{\left(\frac{C_m V_{pmax}}{C_m + K_p}\right), V_{pr}\right\} \quad \text{Eq. S3.13}$$

where V_{pmax} is the maximum PEP carboxylation rate, K_p is the Michaelis-Menten constant for CO_2, and V_{pr} is a constant representing when PEP regeneration is limiting.

The light- and electron transport-limited photosynthesis rate (A_j) is given by:

$$A_j = min\left\{\left(\frac{xJ}{2} + g_{bs}C_m - 0.5 \cdot R_d\right), \left(\frac{(1-x)J}{3} - R_d\right)\right\} \quad \text{Eq. S3.14}$$

where x is a partitioning factor of the electron transport rate. The electron transport rate (J) is estimated using Eq. S3.4-S3.6, but with J_{max} value of C4 pathway.

Table S3.1. Photosynthetic parameters at 25 °C for C3 and C4 pathways and coefficients to characterize temperature dependency functions.

Parameter	Eqn	Unit	Temperature dependence	Coefficients					
				k_{25}	Q_{10}	E_a (J mol^{-1})	H_a (J mol^{-1})	H_d (J mol^{-1})	S_v (J mol^{-1} K^{-1})
C3 pathway									
I^*	3.2	μmol mol^{-1}	A-fun	42.75	-	37,830	-	-	-
K_c	3.2	μbar	A-fun	404.4	-	79,430	-	-	-
K_o	3.2	mbar	A-fun	278.4	-	36,380	-	-	-
V_{cmax}	3.2	μmol mol^{-1}	P-fun	Table S1	-	-	71,513	200,000	636.29
R_d	3.1	μmol mol^{-1}	P-fun	$0.015V_{cmax}$	-	-	66,400	150650	490
J_{max}	3.4	μmol mol^{-1}	P-fun	$1.54V_{cmax}$	-	-	49,884	200,000	637.2
T_p	3.7	μmol mol^{-1}	P-fun	$0.09V_{cmax}$	-	-	53,100	150650	490
C4 pathway									
K_c	3.10	μbar	A-fun	650	-	-	67,294	-	-
K_o	3.10	mbar	A-fun	450	-	-	36,000	-	-
V_{pr}	3.13	μmol mol^{-1}	Q-fun	80	2.0	-	-	-	-
K_p	3.13	μmol mol^{-1}	Q-fun	80	2.0	-	-	-	-
V_{cmax}	3.11	μmol mol^{-1}	P-fun	Table S1	-	-	67,294	144,568	472
J_{max}	3.4	μmol mol^{-1}	P-fun	$5V_{cmax}$	-	-	77,900	191,929	627
V_{pmax}	3.13	μmol mol^{-1}	P-fun	$1.4V_{cmax}$	-	-	70,373	117,910	376
R_d	3.12	μmol mol^{-1}	P-fun	$0.01V_{cmax}$	-	-	67,294	144,568	472

Across these photosynthesis processes, variables I^*, K_c, K_o, V_{cmax}, V_{pmax} , J_{max}, T_p, R_d, and V_{pr} are temperature dependent, and they are described using three types of dependency functions: 1) Arrhenius function (named as A-fun); 2) peak model function (named as P-fun); and (3) Q10 function (named as Q-fun). They are given respectively by:

$$k_T = k_{25}\mathrm{e}^{E_a\frac{T_l-25}{298(T_l+273)R}} \quad \text{Eq. S3.12}$$

$$k_T = k_{25}\mathrm{e}^{H_a\frac{T_l-25}{298(T_l+273)R}}\frac{1+e^{\frac{298S_v-H_d}{298R}}}{1+e^{\frac{T_lS_v-H_d}{T_lR}}} \quad \text{Eq. S3.13}$$

$$k_T = k_{25}Q_{10}^{\frac{T_l-298}{10}} \quad \text{Eq. S3.14}$$

Where k_{25} is the base rate of k_T at the reference temperature of 25 °C and T_l is leaf temperature in °C. E_a and H_a are both activation energy, H_d is deactivation energy, S_v is entropy term and Q_{10} is the coefficient representing the proportional change in metabolic rate per 10°C increase in temperature, and R is ideal gas constant. The P-fun function is modified from A-fun, and shows the reduction in metabolic rate at high temperatures due to the thermal breakdown of metabolic processes. Table. S3.1 describes this parameterization based on von Caemmerer 2000; Bernacchi et al., 2001; Massad et al., 2007; Kattge et al., 2007; von Caemmerer et al., 2009.

S3.2. Stomatal conductance process

The stomatal conductance model governs the exchange rate of CO_2 and water vapor through leaf stomata, determining the leaf intercellular CO_2 concentration and leaf transpiration rates. Here, an empirical model called Ball-Berry-Leuning model (Ball, Woodrow & Berry 1987; Leuning et al., 1990, 1995) is used to describe both C3 and C4 photosynthetic pathways, and it is given by:

$$g_{sw} = g_0 + \frac{a_1 A_n}{(c_s - \Gamma^*)\left(1 + \frac{D_s}{D_0}\right)} \quad \text{Eq. S3.15}$$

Where g_{sw} is the stomatal conductance to water vapor, g_0 is g_{sw} at CO_2 compensation point, and a_1 and D_0 are empirical coefficients. D_s and c_s are vapor pressure deficit (VPD) and CO_2 partial pressure at the leaf surface. D_s is estimated as:

$$D_s = e_s(T_l) - e_a \quad \text{Eq. S3.16}$$

where e_a is the vapor pressure of ambient air, and $e_s(T_l)$ is saturated vapor pressure at leaf temperature T_l.

The boundary layer conductance of g_{bw} to water vapor is estimated by:

$$g_{bw} = 1.4 \cdot 0.147\sqrt{\frac{u}{d}} = 1.4 \cdot 0.147\sqrt{\frac{u}{0.72w}} \quad \text{Eq. S3.17}$$

where u is wind speed (in unit of m/s) and w is leaf width (m). With the stomatal conductance (g_{sw}) and the boundary layer conductance (g_{bw}), the CO_2 concentration at leaf surface (c_s) and at the leaf intercellular level (c_i) are estimated as:

$$c_s = c_a - \frac{1.4A_n}{g_{bw}} \quad \text{Eq. S3.18}$$

$$c_i = c_s - \frac{1.6A_n}{g_{sw}} \quad \text{Eq. S3.19}$$

where c_a is the CO_2 concentration of ambient air.

S3.3. Leaf energy balance

If heat storage and metabolic heat production are assumed to be negligible, the energy budget of a leaf is:

$$R_{abs} - L_{oe} - H - \lambda E_l = 0 \quad \text{Eq. S3.20}$$

where R_{abs} is the absorbed shortwave and longwave radiation, L_{oe} is emitted thermal radiation, and H and λE are sensible and latent heat loss, respectively. These equations are given by:

$$L_{oe} = \varepsilon_s \sigma {T_l}^4 \quad \text{Eq. S3.21}$$

$$H = c_p g_{ha}(T_l - T_a) \quad \text{Eq. S3.22}$$

$$\lambda E_l = \lambda g_v \frac{e_s(T_l) - e_a}{p_a} \quad \text{Eq. S3.23}$$

Where ε_s is leaf thermal emissivity, σ is the Stefan-Boltzmann constant, c_p is specific heat capacity of air, T_a is the air temperature, and E is the transpiration rate. g_{ha} and g_v are heat conductance and vapor conductance, respectively, and are given by:

$$g_{ha} = 1.4 \cdot 0.135\sqrt{\frac{u}{0.72w}} \quad \text{Eq. S3.24}$$

$$g_v = 0.5\frac{g_{sw}g_{bw}}{g_{sw} + g_{bw}} \quad \text{Eq. S3.25}$$

S3.4. Coupling and solving three processes

The three processes of photosynthesis, stomatal conductance, and leaf energy balance are interdependent. The process of photosynthesis requires leaf temperature (T_l) and leaf intercellular CO_2 concentration (c_i) as inputs, and subsequently offers the net carbon assimilation rate (A_n) as one of its outputs. The stomatal conductance process requires T_l and A_n as inputs, and delivers estimates of c_i and g_{sw} as outputs. The leaf energy balance process requires g_{sw} as an input and in turn provides an estimate of T_l. Therefore, all three processes are solved in numerical iteration. First, A_n is obtained when photosynthesis is initialized by setting T_l and c_i at air temperature T_a and $0.7c_a$, respectively. Second, A_n is used in the stomatal conductance process to update c_i. Steps one and two are solved using the Newton-Raphson method until the c_i is converged upon. Third, the c_i and g_{sw} from the steps one and two are used in the leaf energy balance process to solve T_l. These three steps are iterated until T_l is converged upon. As a result, the net carbon assimilation rate (A_n) and transpiration rate (E_l) are scaled up to the canopy-level and drive the growth process in other submodules.

S3.5. Water and nitrogen constraint

Net photosynthesis in Eq. S3.1 and Eq. S3.8 and transpiration rates in Eq. S3.23 are modelled without accounting for stress from soil moisture and nitrogen availability. However, low availability of water and nitrogen could decrease photosynthesis and transpiration by limiting stomatal conductance (g_{sw}), photosynthetic capacity (V_{cmax}), or both. Following Moorcroft et al., 2001, the net photosynthesis rate, $A_n(\mathbf{r}, t, c^*)$ and transpiration rate, $E_l(\mathbf{r}, t, c^*)$ are adjusted for water and nitrogen stress using a simple approach:

$$A_n(\mathbf{r}, t, c^*) = c^* A_n + (1 - c^*){A_n}^c \quad \text{Eq. S3.26}$$

$$E_l(\mathbf{r}, t, c^*) = c^* E_l + (1 - c^*){E_l}^c \quad \text{Eq. S3.27}$$

$$c^* = f_w f_N \quad \text{Eq. S3.28}$$

where ${A_n}^c$ and ${E_l}^c$ are net photosynthesis and transpiration when fully constrained, assuming equal to A_n and E_l at zero light input. c^* is the combined stress factor of water limitation f_w and nitrogen limitation f_N. f_w and f_N are calculated based on the ratio of water/nitrogen uptake by fine roots and that demanded by leaves. Fine root uptake is controlled by fine root biomass, the availability of water, and mineralized nitrogen in soil. f_w and f_N are equal to 0 when demand exceeds supply and set to 1 if there is no limitation in supply.

S4. Leaf phenology and freezing submodule

The total leaf area of a cohort is dynamic, resulting not only from prior carbon balance and allocation but also environmental conditions (i.e., temperature and soil water availability). Three types of dynamic phenology are considered in the model, including evergreens, where the leaves remain year-around; drought-deciduous, where leaves are reduced if soil water drops below a critical threshold (W_{crit}); and cold-deciduous, where leaves are reduced if air temperature is below a PFT-dependent threshold ($T_{crit}(\mathbf{x})$ in Table S1.1). When either drought- or cold- deciduous phenology is triggered, leaf biomass (B_l) is set at zero. A fraction of lost leaf biomass (defined as L_frac) is relocated to a non-respiring, non-decaying, and non-photosynthetic pool called virtual leaf biomass B_{lv}. The remaining biomass fraction (1- L_frac) is then added to the litter pools where the associated carbon and nitrogen will be cycled within the belowground biochemical submodule. The virtual leaf biomass (B_{lv}) is accounted for within B_a but does not lead to photosynthesis and respiration. When both soil water and air temperatures are favourable, leaf biomass B_l recovers instantly to a level depending on remaining B_a and allometry (for further details see the allocation submodule).

Exposure to low temperatures can cause tissue damage to twigs and buds, affecting subsequent carbon balance and survival (DeHayes, 1992; Gu et al., 2008; Sakai and Larcher, 2012; Sakai and Weiser, 1973; Vitasse et al., 2014). Injury effects are characterized by introducing leaf loss at low temperatures. For cold-deciduous PFTs, freezing injury will occur if the monthly average air temperature continues to drops below the defined PFT-specific threshold of resistance ($T_{free}(\mathbf{x})$ in Table S1.1), the virtual leaf biomass by L_frac, which is added to litter pools. Loss of virtual leaf biomass reduces B_a accordingly, in turn affecting the amount of leaf biomass can be recovered when air temperature returns to a favourable level. The resulting leaf loss could affect ongoing carbon assimilation and height growth, and also may result in competitive disadvantage over others PFTs with more resistance to freezing.

S5. Growth submodule

The growth submodule follows Moorcroft et al., 2001 and provides the growth function for $g_a(\boldsymbol{z}, \mathbf{x}, \bar{r}, t)$ and $g_s(\boldsymbol{z}, \mathbf{x}, \bar{r}, t)$, as a result of the carbon balance between carbon assimilation and respiration. Plants gain carbon through leaf photosynthesis and lose carbon by respiration and decay of leaves and roots (decay and respiration of sapwood and structural tissues are assumed to be negligible), and devote remaining carbon to production and growth of active and structural tissue. This process of net carbon production ($Prod$) is given by:

$$Prod = A(\mathbf{r}, t, c^*) l(\mathbf{x}) B_l - R_d l(\mathbf{x}) B_l - \beta_r(\mathbf{x}) B_r f(T_s) - \alpha_l(\mathbf{x}) B_l - \alpha_r(\mathbf{x}) B_r \quad \text{Eq. S5.1}$$

On the right-hand side of the equation, the first term represents total gross carbon fixation by all leaves, the second and third terms represent biomass and temperature dependent respiration of leaves and fine roots, respectively. The last two terms, representing decay of leaves and fine roots, are only related to biomass. $A(\mathbf{r}, t, c^*)$ and R_d are the gross photosynthesis rate and leaf respiration per unit leaf area given resource **r** (light, water, CO_2) and soil water stress (c^*) at time t. $l(\mathbf{x})$ is specific leaf area (SLA), β_r is the respiration coefficient for fine root, and $f(T_s)$ is the dependence function of respiration on soil temperature (T_s). α_l and α_r are the decay rates of leaves and fine roots, respectively, with values reciprocal to longevity.

The net carbon production ($Prod$) can be positive or negative depending on environmental conditions and leaf conditions. This variability results in several cases where carbon is differentially partitioned among the growth of active tissues, structural tissues, and reproduction. When $Prod$ is positive:

$$g_a(\boldsymbol{z}, \mathbf{x}, \bar{r}, t) = Prod \cdot [1 - rp(\mathbf{x})] \cdot q_a(\boldsymbol{z}, \mathbf{x}) \quad \text{Eq. S5.2}$$

$$g_s(\boldsymbol{z}, \mathbf{x}, \bar{r}, t) = Prod \cdot [1 - rp(\mathbf{x})] \cdot [1 - q_a(\boldsymbol{z}, \mathbf{x})] \quad \text{Eq. S5.3}$$

$$RP(\boldsymbol{z}, \mathbf{x}, \bar{r}, t) = Prod \cdot rp(\mathbf{x}) \quad \text{Eq. S5.4}$$

where $rp(\mathbf{x})$ defines the fraction of $Prod$ used for reproduction, $q_a(\boldsymbol{z}, \mathbf{x})$ represents the fraction of new growth devoted to active tissues B_a (calculated in Eq. S2.11), and $RP(\boldsymbol{z}, \mathbf{x}, \bar{r}, t)$ is total carbon allocated for new seedlings (see more details in S6 on the reproduction submodule). A positive $Prod$ represents situations where a plant's carbon fixation from photosynthesis is sufficient for growth and reproduction, even after deducting carbon losses due to respiration and decay.

In contrast, negative $Prod$ occurs when environmental conditions do not favour photosynthesis (e.g., dry air forces leaf stomata closed) or when leaf drop is triggered by soil water stress or low air temperatures. In this case:

$$g_a(\boldsymbol{z}, \mathbf{x}, \bar{r}, t) = Prod \quad \text{Eq. S5.5}$$

$$g_s(\boldsymbol{z}, \mathbf{x}, \bar{r}, t) = 0 \quad \text{Eq. S5.6}$$

$$RP(\boldsymbol{z}, \mathbf{x}, \bar{r}, t) = 0 \quad \text{Eq. S5.7}$$

where all of $Prod$ is used for the plant's active tissue.

S6. Reproduction submodule

Plants in positive carbon balance maintain enough carbon $RP(\mathbf{z}, \mathbf{x}, \bar{r}, t)$ to reproduce seedings. The fecundity $F(\mathbf{z}, \mathbf{x}, a, t)$ is calculated as:

$$F(\mathbf{z}, \mathbf{x}, a, t) = \frac{RP(\mathbf{z}, \mathrm{x}, \bar{r}, t)}{B_{a0} + B_{s0}}(1 - \lambda_{SD}) \quad \text{Eq. S6.1}$$

where B_{a0} and B_{s0} are the initial active and structural biomass of a seedling with functional type **x**, and $1 - \lambda_{SD}$ is the probability of seeding survivorship (λ_{SD} = 0.95). The dead seedlings will be loaded into the soil pools for later carbon and nitrogen decomposition.

Seedling dispersal includes local dispersal, which limits seedlings to the siting patch (i.e. local patch), and non-local dispersal, which distributes seedlings to all other patches. Thus, for any patch, it will receive seedlings not only from all plants of different sizes in its own cohorts but also from plants in other patches. Dispersed seedlings will form a new cohort at the local patch, where plant individual density of the new cohort is represented as:

$$n_i(z_0, \mathbf{x}, a, t) = \frac{1}{G_0}\int_0^\infty F(\mathbf{z}, \mathbf{x}, a, t)\, n_i(\mathbf{z}, \mathbf{x}, a, t)(1 - m(\mathbf{x}))\, d\mathbf{z} + \frac{1}{G_0}\frac{1}{p_i(a, t)}\int_0^\infty \int_0^\infty F(\mathbf{z}, \mathbf{x}, a, t)\, n_i(\mathbf{z}, \mathbf{x}, a, t) p_i(a, t) m(\mathbf{x})\, da\, d\mathbf{z} \quad \text{Eq. S6.2}$$

where $m(\mathbf{x})$ is the PFT-dependent non-local dispersal rate, representing the fraction of plant seedings that will be dispersed to other non-local patches. The first term on the right-hand side of the equation represents seedlings received from all cohorts within the local patch, and the second term represent seedlings from non-local patches.

S7. Mortality submodule

The plant mortality rate $\mu(\boldsymbol{z}, x, \bar{r}, t)$ includes density-independent $\mu_{DI}(\mathrm{x})$ and density-dependent $\mu_{DD}(z, \mathrm{x}, \bar{r}, t)$ components, where:

$$\mu(\mathbf{z}, \mathrm{x}, \bar{r}, t) = \mu_{DI}(\mathrm{x}) + \mu_{DD}(z, \mathrm{x}, \bar{r}, t) \quad \text{Eq. S7.1}$$

The density-independent $\mu_{DI}(\mathbf{x})$ component is related to disturbance, wood density, and life-history of a PFT, such that $\mu_{DI}(\mathbf{x})$ is the sum of disturbance related ($\mu_{DI-DIS}(\mathbf{x})$) and wood-density related ($\mu_{DI-\rho}(\mathbf{x})$) components. $\mu_{DI-\rho}(\mathbf{x})$ varies by PFT. For example, in comparison to the late-successional broadleaf PFT, the early- and mid-successional broadleaf PFTs have relatively higher rates of carbon accumulation and lower wood densities, making them susceptible to pathogen attack and to windthrow disturbance. Thus, $\mu_{DI-\rho}(\mathbf{x})$ decreases for early- to mid- and late-successional PFTs. In addition, the tropical variant of the broadleaf PFTs, has higher $\mu_{DI-\rho}(\mathbf{x})$ than the non-tropical variant. $\mu_{DI}(\mathbf{x})$ for each PFT (as shown in Table. S1.1).

The density-dependent $\mu_{DD}(z, \mathbf{x}, \bar{r}, t)$ component of plant mortality is related to the averaged carbon balance over a given historical period. This component is calculated as:

$$\mu_{DD}(z, \mathbf{x}, \bar{r}, t) = \frac{10}{1 + e^{20 \frac{\int_{t-\Delta t}^{t} Prod(t)dt}{\int_{t-\Delta t}^{t} Prod_{FS}(t)dt}}} \quad \text{Eq. S7.2}$$

where $\int_{t-\Delta t}^{t} Prod(t)dt$ is the cumulative carbon balance of a plant from time $t - \Delta t$ to t, and $\int_{t-\Delta t}^{t} Prod_{FS}(t)\,dt$ is the cumulative carbon balance of the plant under full sun conditions. $\mu_{DD}(z, \mathbf{x}, \bar{r}, t)$ is a nonlinear function of light competition, namely shading from other plants could result in an increased mortality rate.

S8. Soil biogeochemical submodule

The soil biogeochemical submodule tracks belowground carbon and nitrogen dynamics using a simplified Century model (Parton, 1996). This submodule primarily follows Moorcroft et al., 2001. For each patch, three carbon pools are tracked including the structural litter carbon pool $C_1(a,t)$, metabolic litter carbon pool $C_2(a,t)$ and soil slow carbon pool $C_3(a,t)$. By assuming nitrogen is mostly bonded in carbon, nitrogen dynamics have the same three pools as carbon plus a mineralized nitrogen pool which stores nitrogen in plant-available forms (nitrate and ammonium).

Decaying tissues from living plants, and active and structural tissues of dead plants are loaded into structural and metabolic litter carbon pools $C_1(a,t)$ and $C_2(a,t)$. A fraction of both decaying active tissues and dead plant active tissue enter $C_1(a,t)$, with the rest entering $C_2(a,t)$. Two litter pools decompose the carbon under different decomposition rates; both pools depend on defined intrinsic decomposition rates and soil moisture, but the decomposition rate of structural pool is additionally controlled by lignin content in the pool. All decomposed carbon from the metabolic litter pool and part of that from the structural litter pool is lost due to heterotrophic respiration (RH). The rest of the carbon from the structural litter pool is transported to the slow soil carbon pool, where its decomposed at a relative slower rate. Thus, at time t, change rates of structural, metabolic litter and slow soil carbon pools are given:

$$\frac{dC_1(a,t)}{dt} = C_{1,decay}(r,a,t) + C_{1,dead}(r,a,t) - C_{1,decomp}(r,a,t) \quad \text{Eq. S8.1}$$

$$\frac{dC_2(a,t)}{dt} = C_{2,decay}(r,a,t) + C_{2,dead}(r,a,t) - C_{2,decomp}(r,a,t) \quad \text{Eq. S8.2}$$

$$\frac{dC_3(a,t)}{dt} = (1 - r_{stsc})C_{1,decomp}(r,a,t) - C_{3,decomp}(r,a,t) \quad \text{Eq. S8.3}$$

Where $C_{1,decay}(r,a,t)$ and $C_{1,dead}(r,a,t)$ represent the carbon loaded to the structural litter carbon pool from decaying tissues of living plants, and active and structural tissues from dead plants and seedlings, respectively, $C_{1,decomp}(r,a,t)$ is decomposed carbon from the structural litter carbon pool. $C_{2,decay}(r,a,t)$ and $C_{2,dead}(r,a,t)$ represent carbon loaded into the metabolic litter carbon pool from decaying tissues of living plants, and active and structural tissues from dead plants seedlings, respectively. $C_{2,decomp}(r,a,t)$ is decomposed carbon from the metabolic litter carbon pool. Decomposition rates for the three pools are calculated as:

$$C_{1,decomp}(r,a,t) = A\big(a,t,T_s,W(a,t)\big)K_1 e^{-3L_s}C_1(a,t) \quad \text{Eq. S8.4}$$

$$C_{2,decomp}(r,a,t) = A\big(a,t,T_s,W(a,t)\big)K_2 C_2(a,t) \quad \text{Eq. S8.5}$$

$$C_{3,decomp}(r,a,t) = A\big(a,t,T_s,W(a,t)\big)K_3 C_3(a,t) \quad \text{Eq. S8.6}$$

where $A\big(a,t,T_s,W(a,t)\big)$ is a combined factor (ranging from 0-1) of soil temperature and moisture, K_1, K_2 and K_3 are constant coefficients, and L_s is the relative fraction of lignin in the structural carbon pool. Together with Eq. S8.1, S8.2 and S8.3, the total heterotrophic respiration at time *t* is calculated as:

$$R_h(a,t) = r_{stsc}C_{1,decomp}(r,a,t) + C_{2,decomp}(r,a,t) + C_{3,decomp}(r,a,t) \quad \text{Eq. S8.7}$$

Nitrogen pools include the structural litter nitrogen pool $N_1(a,t)$, metabolic litter nitrogen pool $N_2(a,t)$, soil slow nitrogen pool $N_3(a,t)$, and mineralized nitrogen pool $N_4(a,t)$. Nitrogen is assumed to largely be bonded with carbon. The carbon to nitrogen ratio is fixed at 150 for the structural litter pool and 10 for the soil slow pool but floating for the metabolic pool depending on the PFT's leaf nitrogen content. Nitrogen dynamics across pools are similar to carbon dynamics, except that the nitrogen attached to carbon lost during heterotrophic respiration is assumed to be mineralized, and subsequently added to the mineralized nitrogen pool $N_4(a,t)$:

$$\frac{dN_1(a,t)}{dt} = N_{1,decay}(r,a,t) + N_{1,dead}(r,a,t) - N_{1,immbo}(r,a,t) \quad \text{Eq. S8.8}$$

$$\frac{dN_2(a,t)}{dt} = N_{2,decay}(r,a,t) + N_{2,dead}(r,a,t) - N_{2,min}(r,a,t) \quad \text{Eq. S8.9}$$

$$\frac{dN_3(a,t)}{dt} = N_{1,immbo}(r,a,t) - N_{3,min}(r,a,t) \quad \text{Eq. S8.10}$$

$$\frac{dN_4(a,t)}{dt} = N_{2,min}(r,a,t) + N_{3,min}(r,a,t) - N_{up}(r,a,t) - N_{lea}(r,a,t) \quad \text{Eq. S8.11}$$

Where $N_{1,decay}(r,a,t)$ and $N_{1,dead}(r,a,t)$ are nitrogen inputs into the structural litter nitrogen pool from decaying tissues of living, and active and structural tissue from dead plants and seedlings, respectively. $N_{1,immbo}(r,a,t)$ is decomposed nitrogen which will be transported to the soil slow nitrogen pool. $N_{2,decay}(r,a,t)$ and $N_{2,dead}(r,a,t)$ are nitrogen inputs to the metabolic litter nitrogen pool from either the decaying tissue of living plants and seedings or the active and structural tissue from them once dead. $N_{2,min}(r,a,t)$ and $N_{3,min}(r,a,t)$ are mineralized nitrogen from the metabolic litter and soil slow pools, and $N_{up}(r,a,t)$ is nitrogen uptake by plants. $N_{lea}(r,a,t)$ is leached nitrogen, which is assumed to be linearly related to the percolation and runoff rate $perc(a,t)$ which is calculated in hydrology submodule. Nitrogen flows in the above equations are calculated stoichiometrically as a product of the corresponding carbon flow and carbon to nitrogen ratio.

S9. Hydrology submodule

The hydrology submodule tracks incoming soil water flow from precipitation and snow melt and outgoing flow through percolation, runoff, and evapotranspiration from the soil and plant canopy. At time t, soil water change rate is given by:

$$\frac{dW(a,t)}{dt} = P(a,t) + SM(a,t) - perc(a,t) - E_{soil,canopy}(a,t) - W_{up}(a,t) \quad \text{Eq. S9.1}$$

where $W(a,t)$ is soil water availability, $P(a,t)$ and $SM(a,t)$ are incoming water flux from snowmelt, and $perc(t)$ is water loss due to percolation and runoff, $E_{soil,canopy}(a,t)$ is water loss due to evaporation from the soil and canopy, and $W_{up}(a,t)$ is plant water uptake for transpiration.

$W_{up}(a,t)$ equals the total transpiration of all leaves:

$$W_{up}(a,t) = \int_0^\infty E_l(\mathbf{r},t,c^*) l(\mathbf{x}) B_l n_i(\mathbf{z},\mathbf{x},a,t)\, d\mathbf{z} \quad \text{Eq. S9.2}$$

where $E_l(\mathbf{r},t,c^*)$ is the leaf transpiration rate per leaf area, given in the leaf physiology submodule.

When the monthly average air temperature drops below the freezing point, precipitation falls as snow to accumulate snowpack; no water is loaded into the soil. When the monthly average air temperature rises above the freezing point, precipitation falls as rain and snowpack start to melt at a rate linearly related to air temperature until depletion; both precipitation and snowmelt are loaded into the soil. The snowmelt and snowpack change rate is given by:

$$\frac{dSP(a,t)}{dt} = P_s(a,t) - SM(a,t) \quad \text{Eq. S9.3}$$

$$SM(a,t) = \begin{cases} 0, & T_a < 0°\text{C or } SP(a,t) = 0 \\ T_a k_{melt}, & T_a \geq 0°\text{C and } SP(a,t) > 0 \end{cases} \quad \text{Eq. S9.4}$$

where $SP(a,t)$ is snowpack, $P_s(a,t)$ equals to $P(a,t)$ when air temperature is below the freezing point and otherwise equal to zero. k_{melt} is the coefficient constant of the melting rate, set at $100\ mm\ °\text{C}^{-1}\ month^{-1}$. Snowmelt ceases when cumulated snowpack is depleted.

Percolation and runoff rate $perc(a,t)$ is related to hydraulic conductivity, which is a nonlinear function of soil water availability. This relationship is given as:

$$perc = K_{sat,MvG} S_e(a,t)^{L_{MvG}} \left(1 - \left(1 - S_e(a,t)^{\frac{1}{m_{MvG}}}\right)^{m_{MvG}}\right)^2 \quad \text{Eq. S9.5}$$

$$S_e(a,t) = \frac{\frac{W(a,t)}{d_{soil}} - \theta_{res,MvG}}{\theta_{sat,MvG} - \theta_{res,MvG}} \quad \text{Eq. S9.6}$$

Where $K_{sat,MvG}$ is saturated hydraulic conductivity, $\theta_{res,MvG}$ and $\theta_{sat,MvG}$ are residual and saturated volumetric water content. $S_e(a,t)$ is effective volumetric saturation, d_{soil} is soil depth (in mm). L_{MvG} and m_{MvG} are Mualem–van Genuchten (MvG) coefficients (van Genuchten, 1980), specified by gridded soil hydraulic data external to ED (e.g. Montzka et al., 2017).

Evaporation from the soil and canopy is estimated using a model developed by Mu et al., 2011, with the sum represented as:

$$E_{soil,canopy}(a,t) = E_{canopy}(a,t) + E_{soil}(a,t) \quad \text{Eq. S9.7}$$

Both $E_{soil}(a,t)$ and $E_{canopy}(a,t)$ are estimated based on the Penman-Monteith (P-M) equation (Monteith, 1965):

$$\lambda E = \frac{s \cdot R + \frac{\rho \cdot c_p \cdot (e_{sat} - e)}{r_a}}{s + \gamma \cdot \left(1 + \frac{r_s}{r_a}\right)} \quad \text{Eq. S9.8}$$

Where s is slope of the curve relating saturated water vapor pressure (e_{sat}) to temperature, R is available energy partitioned between sensible heat, latent heat, and soil heat fluxes, ρ is air density, c_p is the specific heat capacity of air, γ is the psychrometric constant, r_a is aerodynamic resistance, r_s is an effective resistance to evaporation from the land surface. Calculations of r_a and r_s are different for soil and canopy.

Canopy evaporation ($E_{canopy}(a,t)$) comes from wet canopy which intercepts precipitation. Based on the P-M equation, $E_{canopy}(a,t)$ is given by:

$$E_{canopy}(a,t) = \frac{1}{\lambda} \frac{\left[s \cdot R_{canopy} + \frac{\rho \cdot c_p \cdot (e_{sat} - e)}{rhrc}\right] \cdot F_c \cdot F_{wet}}{s + \frac{P_a \cdot c_p \cdot rvc}{\lambda \cdot \varepsilon \cdot rhrc}} \quad \text{Eq. S9.9}$$

where R_{canopy} is part of R in Eq. S9.8 allocated to canopy, F_c is the patch fraction covered by plants, and F_{wet} is the wet fraction of the land surface, correlated to air relative humidity (Fisher et al., 2008). $rhrc$ and rvc are aerodynamic resistance and wet canopy resistance to evaporation from wet canopy. Calculation of F_c, R_c, F_{wet}, $rhrc$, and rvc can be found in Mu et al., 2011.

Soil evaporation $E_{soil}(a,t)$ consists of potential evaporation from both the saturated soil surface and moist soil surface, thereby $E_{soil}(a,t)$ equals to:

$$E_{soil}(a,t) = E_{wet\_soil}(a,t) + E_{pot\_soil}(a,t)\left(\frac{e_{sat} - e}{100}\right)^{(e_{sat}-e)/200} \quad \text{Eq. S9.10}$$

Then $E_{wet\_soil}(a,t)$ and $E_{pot\_soil}(a,t)$ are estimated as:

$$E_{wet\_soil}(a,t) = \frac{1}{\lambda} \frac{\left[s \cdot R_{soil} + \frac{\rho \cdot c_p \cdot (1 - F_c) \cdot (e_{sat} - e)}{ras}\right] \cdot F_{wet}}{s + \frac{\gamma \cdot rtot}{ras}} \quad \text{Eq. S9.11}$$

$$E_{pot\_soil}(a,t) = \frac{1}{\lambda} \frac{\left[s \cdot R_{soil} + \frac{\rho \cdot c_p \cdot (1 - F_c) \cdot (e_{sat} - e)}{ras}\right] \cdot (1 - F_{wet})}{s + \frac{\gamma \cdot rtot}{ras}} \quad \text{Eq. S9.12}$$

Where R_{soil} is the portion of R in Eq. S9.8 allocated to the soil surface, ras is the aerodynamic resistance at the soil surface, and $rtot$ is the sum of the soil surface resistance and aerodynamic resistance to water vapor transport. Calculation of ras and $rtot$ is related to air temperature, and further details can be found in Mu et al., 2011.

$E_{soil}(a,t)$ and $E_{canopy}(a,t)$ are calculated separately for day and night, using the same equations but different parameter values. The sum of both day and night evaporation is then weighted by the daytime fraction.

S10. Disturbance and fire submodule

The disturbance submodule describes the impacts of natural disturbance (treefall, hurricane, and fire) on patch and cohort dynamics as well as the associated carbon cycle. Disturbance impact on patch demography has been depicted in the patch dynamic PDE equation, where the second term on the right-hand side denotes changes in the proportion of patch natural disturbance. Currently three types of disturbance are included: treefall, hurricane, and fire. The disturbance rate $\boldsymbol{\lambda_i(a,t)}$ is given by:

$$\lambda_i(a,t) = max\left(\lambda_{treefall} + \lambda_{hurricane}, \lambda_{fire}(a,t)\right) \quad \text{Eq. S10.1}$$

Where $\boldsymbol{\lambda_{treefall}}$ is set as 0.014 yr^{-1} and 0.012 yr^{-1} for tropical and non-tropical regions, respectively. $\boldsymbol{\lambda_{hurricane}}$ is specified either by an internal parameter or via external data. $\boldsymbol{\lambda_{fire}(a,t)}$ is either calculated within the fire submodule or specified by external data.

Disturbance reduces the area of all patches proportionally and then forms a new patch. The boundary conditions of area and carbon, nitrogen and water pools for this new patch are represented as:

$$p_i(0,t) = \int_0^\infty \lambda_i(a,t) p_i(a,t)\, da \quad \text{Eq. S10.2}$$

$$PL_i(0,t) = \int_0^\infty PL_i(a,t) \frac{\lambda_i(a,t) p_i(a,t)}{p_i(0,t)} da \quad \text{Eq. S10.3}$$

where PL represents each pool of soil carbon, nitrogen, and water. As the above two equation shows, the new patch proportionally inherits pools from the source patches.

In addition to area and pool changes, disturbance also removes a fraction of the plants within involved patches. Some plants from the reduced patch area survive the disturbance and are relocated to the new patch; the rest of plants die and their carbon and nitrogen are loaded into the soil pools. The individual density of surviving plants is represented as:

$$n_i(\mathbf{z},\mathbf{x},0,t) = \int_0^\infty S(\mathbf{x}) n_i(\mathbf{z},\mathbf{x},a,t) \lambda_i(a,t)\, da \quad \text{Eq. S10.4}$$

where $S(\mathbf{x})$ is survivorship dependent on the disturbance and PFT type. For non-fire related disturbance (i.e., treefall or hurricane), survivorship is differentiated by tree height. Thereby $S(\mathbf{x})$ is given by:

$$S(\mathbf{x}) = \begin{cases} s_{lt}(\mathbf{x}), & h(\mathbf{z},\mathbf{x},a,t) < h_{treefall} \\ s_{gt}(\mathbf{x}), & h(\mathbf{z},\mathbf{x},a,t) \geq h_{treefall} \end{cases} \quad \text{Eq. S10.5}$$

Where $h(\mathbf{z},\mathbf{x},a,t)$ is the height of a cohort, $h_{treefall}$ is a defined height threshold, and $s_{lt}(\mathbf{x})$ and $s_{gt}(\mathbf{x})$ are the survivorship rate (scaled from 0 to 1) for a plant with a height above $h_{treefall}$ or below it, respectively. Currently, $s_{lt}(\mathbf{x})$ and $s_{gt}(\mathbf{x})$ are the same for all PFTs, (i.e., values are 1.0 and 0.0, respectively), and $h_{treefall}$ is set as 0, meaning all plants will not survive in treefall disturbance.

For fire-related disturbance, survivorship is different for grasses where:

$$S(\mathbf{x}) = \begin{cases} 1.0, & \mathbf{x} = \text{C3ShG or C4ShG} \\ 0.3, & otherwise. \end{cases} \quad \text{Eq. S10.6}$$

Total carbon of dead plants involved in disturbance is given by:

$$C_{rem,dis}(t) = \int_0^\infty \int_0^\infty [B_a(\mathbf{z},\mathbf{x},a,t) + B_s(\mathbf{z},\mathbf{x},a,t)][1 - S(\mathbf{x})] n_i(\mathbf{z},\mathbf{x},a,t)\lambda_i(a,t) d\mathbf{z}\, da \quad \text{Eq. S10.7}$$

Total carbon of dead plants involved in disturbance is given by:

$$C_{rem,dis}(t) = \int_0^\infty \int_0^\infty [B_a(\mathbf{z},\mathbf{x},a,t) + B_s(\mathbf{z},\mathbf{x},a,t)][1 - S(\mathbf{x})] n_i(\mathbf{z},\mathbf{x},a,t)\lambda_i(a,t) d\mathbf{z}\, da \quad \text{Eq. S10.7}$$

The total carbon of dead plants is partitioned between soil carbon pools and emissions:

$$C_{rem,dis}(t) = \left[1 - C_{rem,dis}(t)\right] C_{rem,dis}(t) + f_{loss} C_{rem,dis}(t) \quad \text{Eq. S10.8}$$

Where the two terms on the right-hand side of the equation represent the carbon partitioned to soil carbon pools and to CO_2 emissions, respectively. f_{loss} is the fraction of carbon lost as emissions. f_{loss} is set as 0.3 for fire-related disturbance (i.e. smoke fraction) and 0 for treefall- and hurricane-related disturbance, which means no carbon will lost as emissions.

Fire disturbance rate $\lambda_{fire}(a,t)$ can be either specified by external burned area data or estimated by the fire submodule (described below). Following Hurtt et al., 2002, fire risk is controlled by fuel and ignition rate, thereby $\lambda_{fire}(a,t)$ is given by:

$$\lambda_{fire}(a,t) = B_{fuel}(a,t) f_{ignition}(a,t) \quad \text{Eq. S10.9}$$

$$B_{fuel}(a,t) = \int_0^\infty \left[B_l(\mathbf{z},\mathbf{x},a,t) + f_{agb} B_{sw}(\mathbf{z},\mathbf{x},a,t) + f_{agb} B_s(\mathbf{z},\mathbf{x},a,t)\right] n_i(\mathbf{z},\mathbf{x},a,t) d\mathbf{z} \quad \text{Eq. S10.10}$$

$$\lambda_{fire}(a,t) = \begin{cases} \left(\frac{\bar{D}}{30000}\right)^{10}, & P(a,t) < 100\ mm\ month^{-1} \\ 0.0, & otherwise. \end{cases} \quad \text{Eq. S10.11}$$

where $B_{fuel}(a,t)$ is total aboveground carbon as fuel, f_{agb} is aboveground ratio of structural biomass B_s, which is set as 0.8. $\bar{D}$ is annual average drought index, calculated from rolling monthly estimates of the number of days precipitation is below potential evapotranspiration rate.

S11. Land use submodule

The land use submodule describes the demographic dynamics of patches and cohorts by tracking the sub-grid heterogeneity associated with different land use types and transitions. A wide range of land use activities are accounted for including deforestation, reforestation, shifting cultivation, and wood harvest. In this submodule, land use activities can alter the demography of patches and cohorts. For example, deforestation for cropland results in an area decrease of forest patches and area increase of new cropland patches, and correspondingly resets the age of affected patches and cohorts. In addition, land use activities alter carbon dynamics, including redistribution of carbon among plant, soil, and wood timber product pools, and legacy effects on the carbon balance such as elevated heterotrophic respiration from dead plants and enhanced carbon sequestration from plant regrowth. Currently, the submodule is structured for use with standard land use forcing from CMIP5 and CMIP6 (i.e., the Land Use Harmonization 1 (LUH1) and 2 (LUH2) datasets) (Hurtt et a., 2011, 2019, 2020). These datasets provide historical gridded land use fractions and transitions between land use types on an annual basis.

Four land use types are characterized: primary land, secondary land, cropland, and pasture. Patches are tagged with a particular land use type (i.e., primary (v), secondary (s), cropland (c), and pasture (p)), and labelled with the corresponding subscript of $p_i(a,t)$ in the Eq. 1 (the core PDE equation for patch dynamic). Transition types among the four land use types are listed in Table. S10.1, along with their corresponding input variables in LUH1 and LUH2. In this table, $\lambda_{\mathrm{v,c}}$, $\lambda_{\mathrm{v,p}}$, $\lambda_{\mathrm{s,c}}$ and $\lambda_{\mathrm{s,p}}$ represent deforestation, $\lambda_{\mathrm{v,s}}$ and $\lambda_{\mathrm{s,s}}$ represent wood harvest, $\lambda_{\mathrm{c,s}}$ and $\lambda_{\mathrm{p,s}}$ represent reforestation. For each grid cell, patch area is subject to:

$$\int_0^\infty p_i(a,t)\,da = \mathrm{LU}_i(t) \qquad (i = \mathrm{v,s,c}\ and\ \mathrm{p}) \tag{Eq. S11.1}$$

where $\mathrm{LU}_i(t)$ is the area of the land use type i at time t, specified by the external land use change dataset (e.g., LUH1 or LUH2).

Land use transitions drive patch demographic changes by reducing the area and land-use proportion of existing patches, which is described as:

$$\frac{\partial}{\partial t}p_i(a,t) = -\frac{\partial}{\partial a}p_i(a,t) - \lambda_i(a,t)p_i(a,t) - \sum_j \lambda_{j,i}(a,t)p_i(a,t) \tag{Eq. S11.2}$$

The above equation has been described in section 2.1, governing patch dynamics in terms of ageing and disturbance due to both natural and anthropogenic land use change. The last term on the right-hand size of the equation represents the patch fraction $p_i(a,t)$ that decreases due to a land use transition from current type *i* to new type *j*. Along with this fractional decrease for all involved patches, a new patch with land use type *j* will be formed. The area, carbon, nitrogen, and water boundary conditions for this new patch are represented as:

$$p_j(0,t) = \sum_i \int_0^\infty \lambda_{j,i}(a,t)p_i(a,t)\,da \qquad (i,j = \mathrm{v,s,c}\ and\ \mathrm{p}) \tag{Eq. S11.3}$$

$$PL_j(0,t) = \sum_i PL_i(0,t)\frac{\int_0^\infty \lambda_{j,i}(a,t)p_i(a,t)\,da}{p_j(0,t)} \qquad (i,j = \text{v, s, c } and \text{ p}) \quad \text{Eq. S11.4}$$

Where PL represents each pool of soil carbon, nitrogen, and water. The above two equations show that the new patch inherits pools from the source patches proportionally.

Depending on the specific transition type, land use transitions may also involve plant removal (Table S10.1). Plant removal will clear native plants and distribute associated carbon to either the wood product or soil litter pools. The carbon from plant removal is partitioned between carbon pools as follows:

$$\begin{aligned} &C_{res,i}(t) \quad \text{Eq. S11.5}\\ &= \int_0^\infty \int_0^\infty [B_a(\mathbf{z},\mathbf{x},a,t)\\ &+ B_s(\mathbf{z},\mathbf{x},a,t)]n_i(\mathbf{z},\mathbf{x},a,t)p_i(a,t)\lambda_{i,j}(a,t)\zeta_{\text{res}}(\mathbf{x},i)\,d\mathbf{z}\,da \qquad (i,j = \text{v, s, c } and \text{ p}) \end{aligned}$$

$$\begin{aligned} \Delta C_{wood,1yr}(t) = \int_0^\infty \int_0^\infty &[B_a(\mathbf{z},\mathbf{x},a,t)\\ &+ B_s(\mathbf{z},\mathbf{x},a,t)]n_i(\mathbf{z},\mathbf{x},a,t)p_i(a,t)\lambda_{i,j}(a,t)[1\\ &- \zeta_{\text{res}}(\mathbf{x},i,j)]\eta_{1yr}(\mathbf{x},i,j)\,d\mathbf{z}\,da \qquad (i,j = \text{v, s, c } and \text{ p}) \end{aligned} \quad \text{Eq. S11.6}$$

$$\begin{aligned} \Delta C_{wood,10yr}(t) = \int_0^\infty \int_0^\infty &[B_a(\mathbf{z},\mathbf{x},a,t)\\ &+ B_s(\mathbf{z},\mathbf{x},a,t)]n_i(\mathbf{z},\mathbf{x},a,t)p_i(a,t)\lambda_{i,j}(a,t)[1\\ &- \zeta_{\text{res}}(\mathbf{x},i,j)]\eta_{10yr}(\mathbf{x},i,j)\,d\mathbf{z}\,da \qquad (i,j = \text{v, s, c } and \text{ p}) \end{aligned} \quad \text{Eq. S11.7}$$

$$\begin{aligned} \Delta C_{wood,100yr}(t) = \int_0^\infty \int_0^\infty &[B_a(\mathbf{z},\mathbf{x},a,t)\\ &+ B_s(\mathbf{z},\mathbf{x},a,t)]n_i(\mathbf{z},\mathbf{x},a,t)p_i(a,t)\lambda_{i,j}(a,t)[1\\ &- \zeta_{\text{res}}(\mathbf{x},i,j)]\eta_{100yr}(\mathbf{x},i,j)\,d\mathbf{z}\,da \qquad (i,j = \text{v, s, c } and \text{ p}) \end{aligned} \quad \text{Eq. S11.8}$$

Where $C_{res,i}(t)$ is removed carbon that is allocated to soil litter pools. $\Delta C_{wood,1yr}(t)$, $\Delta C_{wood,10yr}(t)$ and $\Delta C_{wood,100yr}(t)$ are removed carbon that is allocated to wood product pools with decay rates of 1-year, 10-year and 100-year, respectively. The coefficient $\zeta_{\text{res}}(\mathbf{x},i,j)$ is the carbon fraction left on-site; $\eta_{1yr}(\mathbf{x},i,j)$, $\eta_{10yr}(\mathbf{x},i,j)$ and $\eta_{100yr}(\mathbf{x},i,j)$ are the relative fractions entering each of the three wood product pools. The four coefficients are differentiated among PFTs and between primary or secondary land (Table S10.2), the parameterization is based on Hansis et al. 2015.

In addition to patch dynamics arising from land use transitions, cropland patches are routinely harvested and planted on an annual basis, with planting and harvesting dates specified by an external crop calendar (Sacks et al. 2010). Crop harvesting only leaves a limited number of plants in each patch to ensure reproduction in the following years,

removing all other plants. For pasture patches, grazing is routinely implemented to similarly remove a fraction of plants from each pasture patch. The removed carbon from harvesting and grazing are given by:

$$C_{rem,\mathrm{c}}(t) = \int_0^\infty \int_0^\infty [B_a(\mathbf{z},\mathbf{x},a,t) + B_s(\mathbf{z},\mathbf{x},a,t)]\left[n_{\mathrm{c}}(\mathbf{z},\mathbf{x},a,t) - n_{\mathrm{c,min}}\right] d\mathbf{z}\, da \quad \text{Eq. S11.9}$$

$$C_{rem,\mathrm{p}}(t) = \int_0^\infty \int_0^\infty [B_a(\mathbf{z},\mathbf{x},a,t) + B_s(\mathbf{z},\mathbf{x},a,t)] n_{\mathrm{p}}(\mathbf{z},\mathbf{x},a,t)\lambda_{graz\_inten}\, d\mathbf{z}\, da \quad \text{Eq. S11.10}$$

Where $n_{\mathrm{c,min}}$ is the minimum density of crop plants that are retained post-harvest, λ_{graz_inten} is the grazing intensity which specifies the fraction of plants to be removed due to grazing.

The removed carbon is distributed to the product pools and soil carbon pool, the partitioning of which is given by:

$$C_{rem,\mathrm{c}}(t) = \zeta_{\mathrm{res,c}} C_{rem,\mathrm{c}}(t) + \left(1 - \zeta_{\mathrm{res,c}}\right) C_{rem,\mathrm{c}}(t) \quad \text{Eq. S11.11}$$

$$C_{rem,\mathrm{p}}(t) = \zeta_{\mathrm{res,p}} C_{rem,\mathrm{p}}(t) + \left(1 - \zeta_{\mathrm{res,p}}\right) C_{rem,\mathrm{p}}(t) \quad \text{Eq. S11.12}$$

In above two equations, the first term on the right-hand side of the equation represents on-site plant residuals on cropland or pasture, respectively, these residuals will be loaded into soil litter pools. The second term represents the removed carbon allocated to the product pools of harvested crop and grazed grass. $\zeta_{\mathrm{res,c}}$ and $\zeta_{\mathrm{res,p}}$ are the on-site fraction coefficients, set at 0.5 for cropland and 0.1 for pasture.

Table S11.1. Land use transition types and their corresponding input variables from LUH1 and LUH2. Note *crops* include C3 annual crops (c3ann), C4 annual crops (c4ann), C3 perennial crops (c3per), C4 perennial crops (c4per), and C3 nitrogen-fixing crops (c3nfx). All transitions represent clearing type except primary land harvesting ($\lambda_{v,s}$) and secondary land harvesting ($\lambda_{s,s}$). Clearing and harvesting types have different parameterization for plant removal (see Table S11.2).

Land use transition	LUH1	LUH2	Plant removal
$\lambda_{v,s}$	*gflvh, gflvh2*	*primf_harv, primn_harv*	Y
$\lambda_{v,c}$	*gflvc*	*primf_to_crops, primn_to_crops*	Y
$\lambda_{v,p}$	*gflvp*	*primf_to_pastr, primn_to_pastr primf_to_range, primn_to_range*	Y
$\lambda_{s,s}$	*gfsh1, gfsh2, gfsh3*	*secyf_harv, secmf_harv, secnf_harv*	Y
$\lambda_{s,c}$	*gfsc*	*secdf_to_crops, secdn_to_crops*	Y
$\lambda_{s,p}$	*gflsp*	*secdf_to_pastr, secdn_to_pastr secdn_to_range, secdn_to_range*	Y
$\lambda_{c,s}$	*gflcs*	*crops_to_secdf, crops_to_secdn*	N
$\lambda_{c,p}$	*gflcp*	*crops_to_pastr, crops_to_range*	N
$\lambda_{p,s}$	*gflps*	*pastr_to_secdf, pastr_to_secdn range_to_secdf, range_to_secdn*	N
$\lambda_{p,c}$	*gflpc*	*pastr_to_crops, range_to_crops*	Y

As Eq. S11.6, S11.7, S11.8, S11.11, and S11.12 show, carbon that is partially removed during land use transitions will be allocated to the respective product (e.g., wood, crop, or grass). These pools decay with different rates, for

example, crop and grass pools are assumed to decay immediately, and are lost to the atmosphere as land use emissions. However, wood product pools decay slowly over time with a rate following an exponential curve:

$$\frac{dC_{wood,nyr}(a,t)}{dt} = \Delta C_{wood,nyr}(t) + C_{wood,nyr}(a,t)e^{-\tau_{nyr}dt} \quad \text{Eq. S11.13}$$

Where $C_{wood,nyr}$ is the nyr product pool (nyr=1yr, 10yr, or 100yr), $\Delta C_{wood,nyr}(t)$ is newly loaded carbon due to land use transitions, τ_{nyr} is the coefficient governing the decay rate. This rate is currently set at -1.873, 0.187 and 0.018 for the three wood pools ($C_{wood,1yr}$, $C_{wood,10yr}$ and $C_{wood,100yr}$) respectively, such that three pools reduce to 15% of their respective size within 1 year, 10 years, or 100 years. Decayed carbon from all of three wood product pools contribute to land use emissions.

Table S11.2. Parameters for land use transitions involved in plant removals (i.e.., Eq. S11.5-8)

Parameters	C4ShG	C3ShG	EaSBT, MiSBT, LaSBT		NSP, LaSC
			TRO	NTRO	
Harvesting on primary land					
$\eta_{1yr}(x,v,s)$	1.0	1.0	0.90	0.40	0.40
$\eta_{10yr}(x,v,s)$	0.0	0.0	0.04	0.24	0.24
$\eta_{100yr}(x,v,s)$	0.0	0.0	0.06	0.36	0.36
$\zeta_{res}(x,v,s)$	0.860	0.780	0.825	0.795	0.870
Harvesting on secondary land					
$\eta_{1yr}(x,s,s)$	1.0	1.0	0.90	0.40	0.40
$\eta_{10yr}(x,s,s)$	0.0	0.0	0.04	0.24	0.24
$\eta_{100yr}(x,s,s)$	0.0	0.0	0.06	0.36	0.36
$\zeta_{res}(x,s,s)$	0.810	0.700	0.750	0.725	0.820
Clearing					
$\eta_{1yr}(x,i,j)$	1.0	1.0	0.59	0.59	0.59
$\eta_{10yr}(x,i,j)$	0.0	0.0	0.41	0.31	0.31
$\eta_{100yr}(x,i,j)$	0.0	0.0	0.00	0.10	0.10
$\zeta_{res}(x,i,j)$	0.50	0.50	0.33	0.33	0.33

Reference

Albani, M., Medvigy, D., Hurtt, G. C. and Moorcroft, P. R.: The contributions of land-use change, CO2 fertilization, and climate variability to the Eastern US carbon sink, Global Change Biology, 12(12), 2370–2390, https://doi.org/10.1111/j.1365-2486.2006.01254.x, 2006.

Ball, J. T., Woodrow, I. E., and Berry, J. A.: A model predicting stomatal conductance and its contribution to the control of photosynthesis under different environmental conditions, in: Progress in photosynthesis research, Springer, 221–224, 1987.

Bernacchi, C. J., Singsaas, E. L., Pimentel, C., Jr, A. R. P. and Long, S. P.: Improved temperature response functions for models of Rubisco-limited photosynthesis, Plant, Cell & Environment, 24(2), 253–259, https://doi.org/10.1111/j.1365-3040.2001.00668.x, 2001.

von Caemmerer, S. and Furbank, R. T.: Modeling C4 photosynthesis, C4 plant biology, 173–211, 1999.

von Caemmerer, S.: Biochemical models of leaf photosynthesis, Csiro publishing., 2000.

DeHayes, D. H.: Winter Injury and Developmental Cold Tolerance of Red Spruce, in Ecology and Decline of Red Spruce in the Eastern United States, edited by C. Eagar and M. B. Adams, pp. 295–337, Springer, New York, NY, https://doi.org/10.1007/978-1-4612-2906-3_8, , 1992.

Farquhar, G. D., von Caemmerer, S. and Berry, J. A.: A biochemical model of photosynthetic CO2 assimilation in leaves of C3 species, Planta, 149(1), 78–90, https://doi.org/10.1007/BF00386231, 1980.

Hansis, E., Davis, S. J. and Pongratz, J.: Relevance of methodological choices for accounting of land use change carbon fluxes, Global Biogeochemical Cycles, 29(8), 1230–1246, https://doi.org/10.1002/2014GB004997, 2015.

Hurtt, G. C., Pacala, S. W., Moorcroft, P. R., Caspersen, J., Shevliakova, E., Houghton, R. A. and Moore, B.: Projecting the future of the U.S. carbon sink, PNAS, 99(3), 1389–1394, https://doi.org/10.1073/pnas.012249999, 2002.

Hurtt, G. C., Chini, L. P., Frolking, S., Betts, R., Feddema, J., Fischer, G., Fisk, J., Hibbard, K., Houghton, R., and Janetos, A.: Harmonization of land-use scenarios for the period 1500–2100: 600 years of global gridded annual land-use transitions, wood harvest, and resulting secondary lands, Climatic change, 109, 117–161, 2011.

Hurtt, G., Chini, L., Sahajpal, R., Frolking, S., Bodirsky, B. L., Calvin, K., Doelman, J., Fisk, J., Fujimori, S., Goldewijk, K. K., Hasegawa, T., Havlik, P., Heinimann, A., Humpenöder, F., Jungclaus, J., Kaplan, J., Krisztin, T., Lawrence, D., Lawrence, P., Mertz, O., Pongratz, J., Popp, A., Riahi, K., Shevliakova, E., Stehfest, E., Thornton, P., van Vuuren, D., and Zhang, X.: input4MIPs.CMIP6.CMIP.UofMD, https://doi.org/10.22033/ESGF/input4MIPs.10454, 2019.

Hurtt, G. C., Chini, L., Sahajpal, R., Frolking, S., Bodirsky, B. L., Calvin, K., Doelman, J. C., Fisk, J., Fujimori, S. and Klein Goldewijk, K.: Harmonization of global land use change and management for the period 850–2100 (LUH2) for CMIP6, Geoscientific Model Development, 13(11), 5425–5464, 2020.

Fisher, J. B., Tu, K. P. and Baldocchi, D. D.: Global estimates of the land–atmosphere water flux based on monthly AVHRR and ISLSCP-II data, validated at 16 FLUXNET sites, Remote Sensing of Environment, 112(3), 901–919, 2008.

Gu, L., Hanson, P. J., Post, W. M., Kaiser, D. P., Yang, B., Nemani, R., Pallardy, S. G. and Meyers, T.: The 2007 Eastern US Spring Freeze: Increased Cold Damage in a Warming World?, BioScience, 58(3), 253–262, https://doi.org/10.1641/B580311, 2008.

Kattge, J. and Knorr, W.: Temperature acclimation in a biochemical model of photosynthesis: a reanalysis of data from 36 species, Plant, Cell & Environment, 30(9), 1176–1190, https://doi.org/10.1111/j.1365-3040.2007.01690.x, 2007.

Leuning, R.: Modelling stomatal behaviour and photosynthesis of Eucalyptus grandis, Functional Plant Biology, 17, 159–175, 1990.

Leuning, R.: A critical appraisal of a combined stomatal-photosynthesis model for C3 plants, Plant, Cell & Environment, 18, 339–355, 1995.

Massad, R.-S., Tuzet, A. and Bethenod, O.: The effect of temperature on C4-type leaf photosynthesis parameters, Plant, Cell & Environment, 30(9), 1191–1204, https://doi.org/10.1111/j.1365-3040.2007.01691.x, 2007.

Monteith, J.: Evaporation and environment, Symposia of the Society for Experimental Biology, 19, 205–234, 1965.

Montzka, C., Herbst, M., Weihermüller, L., Verhoef, A. and Vereecken, H.: A global data set of soil hydraulic properties and sub-grid variability of soil water retention and hydraulic conductivity curves, Earth System Science Data, 9(2), 529–543, 2017.

Moorcroft, P. R., Hurtt, G. C. and Pacala, S. W.: A Method for Scaling Vegetation Dynamics: The Ecosystem Demography Model (ed), Ecological Monographs, 71(4), 557–586, https://doi.org/10.1890/0012-9615(2001)071[0557:AMFSVD]2.0.CO;2, 2001.

Mu, Q., Zhao, M., and Running, S. W.: Improvements to a MODIS global terrestrial evapotranspiration algorithm, 115, 1781–1800, 2011.

Parton, W. J.: The CENTURY model, in: Evaluation of soil organic matter models, Springer, 283–291, 1996.

Reich, P. B., Walters, M. B. and Ellsworth, D. S.: From tropics to tundra: Global convergence in plant functioning, Proc Natl Acad Sci USA, 94(25), 13730, https://doi.org/10.1073/pnas.94.25.13730, 1997.

Sacks, W. J., Deryng, D., Foley, J. A. and Ramankutty, N.: Crop planting dates: an analysis of global patterns, Global ecology and biogeography, 19(5), 607–620, 2010.

Sakai, A. and Larcher, W.: Frost Survival of Plants: Responses and Adaptation to Freezing Stress, Springer Science & Business Media., 2012.

Sakai, A. and Weiser, C. J.: Freezing Resistance of Trees in North America with Reference to Tree Regions, Ecology, 54(1), 118–126, https://doi.org/10.2307/1934380, 1973.

Vitasse, Y., Lenz, A. and Körner, C.: The interaction between freezing tolerance and phenology in temperate deciduous trees, Front. Plant Sci., 5, https://doi.org/10.3389/fpls.2014.00541, 2014.

Van Genuchten, M. T.: A closed-form equation for predicting the hydraulic conductivity of unsaturated soils, Soil science society of America journal, 44, 892–898, 1980.

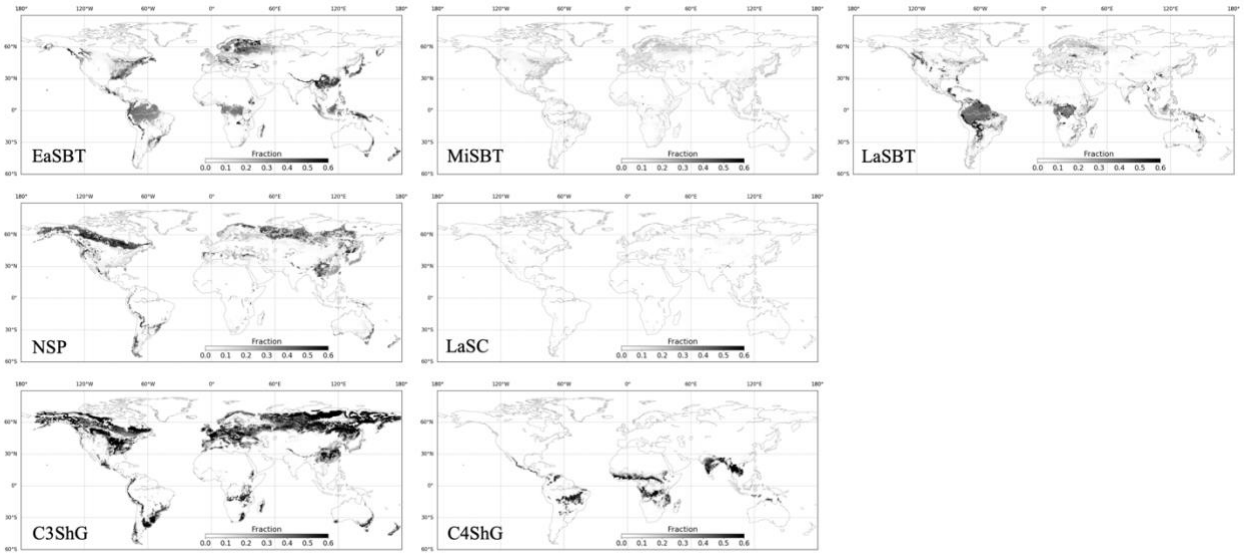

572
573

574 Figure S1. Spatial distribution of seven PFTs from ED.